Hydrol. Earth Syst. Sci. Discuss., 9, 4703–4746, 2012
www.hydrol-earth-syst-sci-discuss.net/9/4703/2012/
doi:10.5194/hessd-9-4703-2012

Hydrology and Earth System Sciences Discussions

Joint statistical correction of clutters, spokes and beam height for a radar climatology in Southern Germany

A. Wagner[1,2,*], **J. Seltmann**[1], **and H. Kunstmann**[2,3]

[1]German Met. Service (DWD), Meteor. Observatory, Hohenpeissenberg, Germany
[2]University of Augsburg, Institute for Geography, Regional Climate and Hydrology, Augsburg, Germany
[3]Karlsruhe Institute of Technology, Institute for Meteorology and Climate Research IMK-IFU, Garmisch-Partenkirchen, Germany
[*]now at: HYDRON GmbH, Karlsruhe, Germany

Received: 19 March 2012 – Accepted: 21 March 2012 – Published: 13 April 2012

Correspondence to: A. Wagner (andreas.wagner@hydron-gmbh.de)

Published by Copernicus Publications on behalf of the European Geosciences Union.

Abstract

Extensive corrections of radar data are a crucial prerequisite for radar derived climatology. This kind of climatology demands a high level of data quality. Little deviations or minor systematic underestimations or overestimations in single radar images become a major cause of error in statistical analysis. First results of radar derived climatology have emerged over the last years, as data sets of appropriate extent are becoming available. Usually, these statistics are based on time series lasting up to ten years as storage of radar data was not achieved before.

We present a new statistical post-correction scheme, which is based on seven years of radar data of the Munich weather radar (2000–2006) that is operated by DWD (German Weather Service). The typical correction algorithms for single radar images, such as clutter corrections, are used. Then an additional statistical post-correction based on the results of a climatological analysis from radar images follows. The aim of this statistical correction is to correct systematic errors caused by clutter effects or measuring effects but to conserve small-scale natural variations in space.

The statistical correction is based on a thorough analysis of the different causes of possible errors for the Munich weather radar. This robust analysis revealed the following basic effects: the decrease of rain rate in relation to height and distance from the radar, clutter effects such as remaining clutter, eliminated clutter or shading effects from obstacles near the radar, visible as spokes, as well as the influence of the Bright Band. The correction algorithm is correspondingly based on these results. It consists of three modules. The first one is an altitude correction, which minimizes measuring effects. The second module corrects clutter effects and the third one realizes a mean adjustment to selected rain gauges. Two different radar products are used. The statistical analysis as well as module one and module two of the correction algorithm are based on frequencies of occurrence of the so-called PX-product with six reflectivity levels. For correction module 3 and for the validation of the correction algorithm rain rates are calculated from the 8-bit-depth so-called DX-product.

HESSD

9, 4703–4746, 2012

An application (2004–2006) and a validation (2007–2009) of this correction algorithm with rain gauges show a much higher conformity for radar climatology after the statistical correction. In the years 2004 to 2006 the Root-Mean-Square-Error (RMSE) decreases from 262 mm to 118 mm excluding those pair of values where the rain gauges are situated in areas of obviously corrupted radar data. The results for the validation period 2007 to 2009 are based on all pairs of values and show a decline of the RMSE from 322 mm to 174 mm.

1 Introduction

The spatio-temporal distribution of precipitation is the central meteorological variable regarding hydrological analyses. Its measuring is very demanding at the same time. Satellite data is still not precise enough whereas its areal coverage is excellent. Point measurements suffer from areal extrapolation errors particularly in cases of precipitation with high variations in space. Weather radar data offers a good compromise between areal rain structure and measuring accuracy. But this is only applicable if a number of influencing factors are being taken into account, which usually leads to certain corrections that have to be made before radar data is processed further (Holleman, 2007). Among the huge number of influencing factors the conversion of radar reflectivity into rain-rate (e.g. Z/R-relationship) is one of the biggest challenges, as it is heavily dependent on dropsize distributions of rain which is usually highly variable in space and time. The influence of the melting layer (Bright Band) with higher radar reflectivities at a certain altitude and lower reflectivities in the snow in higher altitudes was paid only little attention. But during the last years it became a major part of correction of radar data as its influence affects huge parts of the radar image and can exceed the influence of the Z/R-relationship especially in the temperate zone in spring and autumn (e.g. Fabry and Zawadzki, 1995; Franco et al., 2010; Haase et al., 2005; Joss and Lee, 1995; Kitchen et al., 1994; Koistinen, 1991; Krajewski et al., 2010; Sánchez-Diezma et al., 2000; Vignal et al., 1999). Attenuation behind strong convective cells, non-meteorological echoes

HESSD
9, 4703–4746, 2012

like insects, birds, planes, ships and windmills or shading effects behind buildings and mountains are further sources of errors in radar data which have to be paid attention to.

For the analysis of single radar images a thorough usage of correction algorithms usually leads to a good data basis for areal precipitation. Little deviations or small systematic underestimations or overestimations are negligible. But for statistical analysis of a huge number of radar measurements these deviations may become a major cause of error. Especially for extreme rainfall a climatology of radar data seems very promising (Overeem et al., 2010; Pedersen et al., 2008; Rudolph et al., 2011, Wagner et al., 2006). Two ways to deal with this problem are feasible. The first one is to make a great effort in correcting single radar images, like Koistinen et al. (2008) and Overeem et al. (2009) do. The other way, which is presented in this study, uses the usual correction algorithms for single radar images such as Doppler filtering. Additionally, the result of the statistical analysis from radar images is corrected statistically. The aim of this statistical correction is to correct systematic errors caused by insufficiently corrected clutter, influences of shading-effects resulting in spokes in radar images or the deviations caused by increasing beam height and beam width with distance from the radar but to conserve small-scale natural variations in space. The correction algorithm is empirical as very often the reason for a spatial variation is a mixture of several determining factors which cannot be separated. Nevertheless, a thorough analysis of the different causes of deviations and their behaviour in space and time is essential to establish a reliable correction algorithm.

Section 2 gives a brief overview of the investigation area and the different data types used. The main theme and the used method are described in Sect. 3. In Sect. 4 the data basis of the statistical correction is analysed. Deviations in radar images are classified, examined and discussed. These results are the basis for the way the statistical corrections are established. These are described in Sect. 5. Section 6 includes a validation of the correction algorithm using rain gauges.

HESSD
9, 4703–4746, 2012

2 Data

The Munich weather radar is situated 15 km to the North of the city of Munich. The investigation area is a circle of 100 km around the site (see Fig. 1). Annual rain rates range from 700 mm in the northern part of the radar site to 1500 mm at the alpine upland. Even higher rain rates are measured in the Alps. The radar is an operational, dopplerised C-Band weather radar of the German Met. Service with two different scan types: a volume scan which consists of 23 elevations (18 Doppler scans and 5 intensity scans) every 15 min and a near-surface precipitation scan every 5 min. This radar is a very challenging radar site: in the closer vicinity the city of Munich with a number of obstacles decreases radar data quality. To overcome the problem of complete shading an oscillating scan is used. For instance, a few kilometres to the north-east a small ridge necessitates that the angle of radiation has to be increased from 0.8° to 2.1° which results in higher altitudes of the radar beam (see Fig. 1). This oscillation will probably become apparent in the statistical analysis and therefore has to be taken into account for the statistical corrections. In 2006 an optimization of this oscillation was implemented, which also has to be paid attention to. The Munich weather radar was dopplerised in 2004. Since then, a much better clutter suppression (see Fig. 10, top-left panel and Fig. 14, left panel) is in place because of Doppler-filters. Additionally, the range of the Alps leads to clutter and shading effects in the southern part of the radar image.

Two different radar products based on the precipitation scan were used for this analysis. The so-called PX-product with six reflectivity levels (see Table 1) and a spatial resolution of $1 \times 1\,km^2$ has the longest time-series starting in 2000. This radar product for the years 2000 to 2006 is the basis for the analysis of disturbances within the radar image as well as for the development of the correction algorithms. The inner 100 km from the radar site are analysed, which results in a total of 2.4×10^{10} pixel-measurements as a profound basis for a statistical analysis.

HESSD
9, 4703–4746, 2012

The second radar product is the DX-product with 8-bit-depth and the original resolution of 1° in azimuth-direction and 1 km in range. This product is ideal for quantitative purposes and is therefore used for adjustment of radar-data to rain gauges and for means of validation. It is continuously available since 2004.

91 rain gauges in the vicinity of the Munich weather radar with reliable time-series of daily precipitation measurements, at least from 2004 to 2009, were available for the comparison with the radar DX-product. Three groups of rain gauges were established: the first group consists of 33 gauges within a distance from 30 to 60 km from the radar representing the area of the most reliable radar measurements; the second one are 76 rain gauges within the whole radar coverage excluding those which are situated in regions of radar-pixel interpolation like parts of the alpine region or the city of Munich; the third group includes all 91 rain gauges.

Figure 1 gives an overview over the whole investigation area. The mean altitudes for all radar pixel are shown to indicate the consequences of different angles of radiation. Additionally, the locations of the rain gauges are plotted, which are used for the comparison of rain rates between the DX-radar product and the individual rain gauges.

3 Method

Both the analysis of corrupted pixels within radar images of the Munich weather radar and the corrections that are derived from these analyses, are based on the frequency of occurrence of radar reflectivities for each reflectivity level of the PX-product.

The aim of this statistical correction was to improve the results of a statistical analysis of moderate and heavy precipitation such as CONRAD-data (Convection in Radar Products) which is based on the PX-product and focuses on moderate and heavy rain. So the correction of light rain was of minor interest. As the frequency of occurrence of heavy rain was too small to be statistically significant and additionally depends strongly on geographical and meteorological situations, it was not analysed.

HESSD
9, 4703–4746, 2012

The main assumption of this statistical correction is that for light and moderate rain the frequency of occurrence of the associated radar reflectivities should be equal at each point of the radar coverage or equally distributed. Certain geographical characteristics resulting in different meteorological situations with different rain amounts have to be taken into account. Conversely, abrupt variations of frequencies of occurrence in space indicate errors in data basis, so does a general increase or decrease in these frequencies with height or distance from the radar.

The first step of the analysis of corrupted pixels within radar images was to separate regions, which are obviously corrupted by clutter effects, from uncorrupted radar pixels. Visually, a certain area including corrupted pixels of the same source (e.g. mountain clutter) is defined, where uncorrupted pixels form the majority of pixels. Then, histograms of frequencies of occurrence of radar reflectivities were established. The majority of pixels are uncorrupted and form a distinctive peak. So pixels which obviously differ from the distribution of uncorrupted pixels were manually separated. The further separation is realized by the analysis of an empirical distribution of frequencies of occurrence, where its 95 % interval marks the range of uncorrupted pixels. As reflectivity level 1 shows the highest amount of corrupted pixels, the classification for all levels, whether a pixel is falsified or not, is based on level 1.

The uncorrupted radar pixels were analysed for measuring effects, as beam height and beam width increase with distance from the radar. Pixels were classified according to their beam height. Then, the median of the frequency of occurrence of each radar reflectivity level for each altitude class is calculated and plotted against height. In this way, the mean decline of frequency of occurrences with height is further analysed.

For the corrupted radar pixels, three different types of clutter were classified: the “city clutter” of Munich caused by obstacles, “mountain clutter” of the Alps in the South and “spokes” originated from obstacles near the radar. For each clutter type the median of the frequency of occurrence for each radar reflectivity level is compared to the median of the corresponding frequency of occurrence of adjacent undisturbed radar pixels. In

HESSD
9, 4703–4746, 2012

this way, these patterns are analysed with regard to their situation, the circumstances they depend on and the reason for their occurrence.

According to the results of the statistical analysis of the radar images some systematic behaviour was deduced. Two of the three modules of the correction algorithm are closely based on these findings. The first module is an "altitude correction" based on a linear regression model. The second module is the "correction of clutter effects" using derived correction factors or interpolation methods.

The DX-radar-product is used for the comparison of rain amounts from rain gauges to rain amounts from corresponding radar-pixels. It has two objectives: First, a mean bias correction factor is derived from this comparison to adjust mean annual rain rates from radar data to rain rates from rain gauges. This "adjustment" represents the third module of the correction algorithm. Secondly, the comparison with data from rain gauges acts as a quality check for the correction algorithm with an independent data basis (calibration/validation). A perfect match of precipitation amounts derived from radar and precipitation from rain gauges is improbable due to different measuring effects. So, not the characteristics of the whole time-series of precipitation are compared, but only the integral mean annual amount of rain. It is more important that the proportion of the rain amount of a rain gauge close to the radar and at greater distances from the radar is equal to the rain amounts derived from the corresponding radar pixels, than their magnitude is.

A threepart Z/R-relationship is used to calculate rain rate from radar reflectivities of the DX-product (Bartels et al., 2004). This relationship considers the differences of the drop-size-spectra of light, moderate and heavy rain by using three different Z/R-relationships according to radar reflectivity.

Two periods of time were defined for the comparison of rain rates from radar data and rain gauges. The first period from 2004 to 2006 is the period of calibration and adjustment, 2007 to 2009 is the period of validation.

HESSD
9, 4703–4746, 2012

4 Analysis of disturbances in radar images

Figure 2 gives an overview of the frequency of occurrence of radar reflectivities for level 1 (light rain), level 3 (moderate rain) and level 5 (heavy rain). Three main types of clutter disturbances can be found within the vicinity of the Munich weather radar. The first one derives from obstacles of the city of Munich (city clutter) to the south of the radar up to a distance of about 40 km. The second one is the mountain range (mountain clutter) also situated to the south of the radar at ranges of more than 70 km. The third one are spokes resulting from obstacles near the radar. The comparison of these three radar images reveals conspicuous differences of the values of the clutter disturbances. The "uncorrupted" radar pixels show a significant decrease of the frequency of radar reflectivities with height of the radar pixel above ground-level for all radar reflectivities (variations with height).

4.1 Variations with height

The principle of measurement of weather radars emitting a radar beam with a certain angle of radiation and beam width may also cause problems according to the comparability of radar pixels at different distances from the radar. With increasing distance from the radar the radar beam reaches higher altitudes and the radar pixels' volume increase which may lead to differences of rain amounts at different ranges. So the behaviour of the uncorrupted pixels has to be examined in detail, too. The main reasons for possible differences at certain ranges are the measurements at different altitudes. Rainfall is a highly variable meteorological variable in space and time. The highest rain amount can be measured at the bottom of the cloud decreasing with height. Rain with a low vertical extent may lead to only partly beam filling or "overshooting" at greater distances from the radar. Therefore, variations at different ranges from the radar can be deduced from measurement

The aim is not to analyse the small-scale variations but the general mean systematic variations with altitude or distance from the radar. The following figures show the

HESSD
9, 4703–4746, 2012

behaviour of the median of the frequency of occurrence with altitude, separated into classes of height (100 m). The lowest and the highest altitudes should be neglected for the interpretation of the mean behaviour as they only refer to a very small amount of pixels.

Figure 3 gives an overview of the behaviour of the frequency of occurrence of radar reflectivity levels 1, 3 and 5 with height. For level 1 to 3 an increase of the frequency of occurrence of pixels with height becomes obvious below 1 km height; it seems to be very variable. Above 1 km height, a steady decrease of the frequency of occurrence of pixels for light and moderate rain can be observed. For higher reflectivities a decrease for all heights is shown.

For reflectivity level 1 the frequency of occurrence of pixels decreases by 12.9 % per 1 km difference in altitude according to Fig. 3 (left panel) above 1 km height. For higher rain intensities the decrease is even higher but seems to be constant at 20.3 % per 1 km difference in altitude (Fig. 3). Even though the angle of radiation varies to a great extent, the fluctuations of the decrease with height are little and therefore negligible. This result is based on a mixture of different types of rain ranging from strong convective cells to snow. So, a temporal separation into months may display differing results.

Figure 4 shows the same analyses of level 3 but for the months January, April, July and October. The extreme decrease of the frequencies of occurrence in January can be explained by a huge part of low reflectivity levels in snow and a tendency of typically low vertical extensions of rain. Figure 4 for April reveals a remarkable characteristic. The typical decrease of frequencies of occurrence starts after a short increase at 1.5 km altitude. This can be explained by the influence of the melting layer (Bright Band) with higher reflectivities than snow or pure rain. In July the “peak” is shifted to higher altitudes of about two or three kilometres. The frequency of occurrence increases with altitude to a great extent, which can also be explained by the influence of the Bright Band. The figure for October is comparable with April but with a more constant decrease with height.

HESSD
9, 4703–4746, 2012

To indicate the high influence of the melting layer, the areal distribution of the frequency of occurrence of level 3 is shown in Fig. 5. Therefore, the height of the radar beam is reduced to the lowest maximum height for all rays, which is at 2.5 km. So this figure shows the distribution of radar reflectivities with height from the radar site, instead of from the distance or range from the radar site as usually. Especially in April a ring of higher frequencies of occurrence becomes obvious which is typical for a Bright Band. Even though the corresponding pixels are derived at distances ranging from 30 to 50 km because of different angles of radiation a very uniform ring is formed in Fig. 5. So this feature must be a result from a meteorological situation and is not a measuring effect. A distinctive Bright Band is typical for stratiform rain events. The rain clouds must have a certain vertical extension with corresponding radar reflectivities of level 2 or 3 to develop a measureable Bright Band reaching reflectivities which are 10 dBZ or more higher than reflectivities of pure rain. This explains why the Bright Band effects become obvious most clearly at reflectivity level 2 and especially level 3.

Besides the measuring effects the transfer from rain to snow seems to play an important role. As the drop size and its state of aggregation highly vary with time and depend on the air mass and the temperature, two ways to realise a correction seem reasonable. The first one is to correct each single radar image by the vertical profile of reflectivity, which is very sensitive and difficult. The other one is to perform a mean correction for a long period of several years, which is presented here.

4.2 Analysis of clutter effects

The second main cause of error are corrupted pixels caused by clutter effects. Figures 6 and 7 show histograms of the percential difference between the frequency of occurrence of corrupted pixels and the median of uncorrupted pixels of the closer environment for the reflectivity levels 1, 3 and 5 representing the range of light to heavy rain. These histograms allow to highlight the differences of corrupted and uncorrupted pixels even though these differences were already visible in Fig. 2.

HESSD
9, 4703–4746, 2012

4.2.1 City clutter

First, the city clutter is analysed and displayed in Fig. 6. The figure of level 1 (left panel) for city clutter shows a significant influence of clutter with smaller frequencies of occurrence. This is likely due to clutter correction with less correct measurements. For radar reflectivities of higher levels (3 and 5) no further interference of clutter or clutter correction can be observed. So, the city clutter is only dominant for light rain.

4.2.2 Mountain clutter

According to Fig. 7 the mountain clutter seems to have the same characteristics as the city clutter. For low rain intensities clutter is corrected, which results in lower frequencies of occurrence. But for stronger rain the influence of mountain clutter remains extensive. It seems that for level 3 (Fig. 7, middle panel) the influence of clutter is minimized, but it is more likely the remaining clutter and the corrected clutter equalize each other. For level 5 (Fig. 7, right panel) the portion of remaining clutter dominates. It depends on the proportion of the intensity of mountain clutter and the intensity of rain, whether a clutter correction or a higher frequency of occurrence due to signal enhancement by clutter results. So this area of mountain clutter does not represent a reliable data basis for statistical analysis.

4.2.3 Spokes

In Fig. 8 the ten main spokes are analysed (clockwise; starting at 0°). As the contamination of each pixel of one spoke has the same source (which usually is an obstacle near the radar) all affected pixels are regarded combined. So each column of Fig. 8 shows the percential difference between the median of the frequency of occurrence of radar reflectivities of all pixels of one spoke and the median of the corresponding frequencies of unfalsified pixels around. For level 1 a slight underestimation in the sphere of influence of the spokes can be observed. For higher rain amounts the underestimations

HESSD
9, 4703–4746, 2012

are bigger indeed but they stay more or less stable for reflectivity levels 2 to 4 (not all shown here). Only spoke #10 (east-north-east) differs completely from the others. This is not astonishing, as its source is not shading but clutter from airplanes at the Munich airport.

The different behaviours of the frequency of occurrence of radar reflectivities can be explained by the clutter correction. Until 2004 only statistical filters were used to correct clutter. These statistical filters are very rough compared to later correction methods. If clutter is detected, the measurement is very often completely eliminated, which leads to an underestimation of the true frequency of occurrence of pixels.

In February 2004 a new signal processor was installed at the Munich radar site. Since then, Doppler-filtering was available to suppress clutter, which improved data quality significantly. But still clutter effects remain, as the way the Doppler-filtering worked is as follows:

In the so-called CCOR the difference of the amount of clutter and no clutter of the analog channel is calculated and subtracted at the log-channel. This results in clutter for small rain-intensities as the influence of the reflectivity of the obstacle is too big. With increasing rain intensities the influence of clutter may become negligible (cf. city clutter). This is only true for obstacles covering smaller parts of the radar volume. For nearly the entire time-series a constant threshold for clutter of 30 dB was used. This results in a systematic overestimation of reflectivity if the clutter of obstacles exceeds 30 dBZ like Fig. 7 (right panel) reveals. To overcome this problem, variable thresholds based on Fourier algorithms are now used at DWD. If the influence of clutter reaches a certain extent, like for example the Mountain “Zugspitze” with reflectivities of 60–70 dBZ does, calculation of the rain amount is no longer possible. Accordingly, radar pixels behind obstacles are also influenced. Only a certain part of the radar beam intensity reaches these pixels, which results in lower reflectivities as usually. The weakening of the radar beam may reach complete shading. So it is better to use higher angles of radiation and measure at higher altitudes instead, especially if the obstacle is near

HESSD
9, 4703–4746, 2012

the radar. For this reason, the angle of radiation of the Munich weather radar varies between 0.8° in the south-west to 2.1° in the north-east.

5 Correction algorithm

According to the findings in Sect. 3 two main correction types were developed. The first one is the correction of the systematically decrease of frequencies of occurrence of radar reflectivities with height and distance from the radar. The second one is the correction of corrupted pixels like clutter or spokes. As already mentioned, the algorithms are developed for moderate and heavy rain not considering all specifics of light rain. The third correction module is a mean adjustment to rain gauges. The latter is not based on frequencies of occurrence of radar reflectivities from the PX-product but on the comparison of rain rates of rain gauges and the radar DX-product.

5.1 Altitude correction

The altitude correction affects all pixels, even the uncorrupted pixels (see discussion Sect. 2). It was concluded that on a statistical basis only a mean correction is appropriate. According to these results a dependency of the frequency of occurrence of radar reflectivities on the angle of radiation and on the distance from the radar seems probable.

Each reflectivity level is analysed separately. As the angle of radiation varies between 0.8° and 2.1° six mean classes of comparable angles of radiation are build. Above 1 km height, Fig. 3 shows a linear decrease of frequencies of occurrence with height. This indicates that linear regression models may describe this decline best. The aim of the altitude correction is to adjust the frequencies of occurrence of radar reflectivities at each height to one single value which is set to Y_0 (see Eq. 1).

First, the mean inclination m_r (depending on range r) of a linear regression for each reflectivity level and each class of angle of radiation θ was calculated with the distance

HESSD
9, 4703–4746, 2012

r as predictor. Then the relation of this mean inclination with the elevation angle for each level was analysed. The multiplication of this mean inclination with the angle of radiation showed approximately equal results even for reflectivity levels 2 to 5. So the regression equation for the frequencies of occurrence of radar reflectivities Y can be formulated as follows, where Y_0 is the measured frequency of occurrence of radar reflectivities:

$$Y = m_r \cdot r \cdot \theta + Y_0 \tag{1}$$

The altitude h is also a product of distance r and angle of radiation θ:

$$h = \tan(\theta) \cdot r \tag{2}$$

So the regression equation with the mean inclination m_h (depending on height h) can be formulated as follows:

$$Y = m_h \cdot h + Y_0 \tag{3}$$

The correction factor is the quotient of Y_0 and m_h and describes the mean variation of the frequency of occurrence of radar reflectivities with height.

$$f_{\text{cor}} = \frac{Y_0}{m_h} \tag{4}$$

The equation for correcting single pixels can be described by using the height h of each radar pixel:

$$Y_0 = \frac{Y}{(h \cdot f_{\text{cor}} + 1)} \tag{5}$$

For the Munich radar the correction factor is calculated to $f_{\text{cor}} = -20.3$ for moderate and heavy precipitation.

HESSD
9, 4703–4746, 2012

The decrease of the frequency of occurrence of radar reflectivities (level 3) with height of all radar pixels in Fig. 9 (left panel) is compared to only the median of each altitude class (right panel) (same data basis). The variation is similar to the correction factor f_{cor} which is calculated from the regression equation (see Eq. 4). The left image of Fig. 9 reveals a huge dispersion including natural variations of radar reflectivities, but still the decrease of reflectivity detections with height becomes obvious in both figures. The different behaviour of the frequency of occurrence of radar reflectivities with height below 1 km altitude is neglected because of two reasons: First, the effect of the altitude correction near the radar site is small. Second, the entire correction algorithm was established for convective rain-events and heavy rain, where this effect does not occur. So, calculating rain rate from the entire radar measurements will probably result in a slight overestimation of rain rate for altitudes lower than 1 km.

Using the altitude correction for the values in Fig. 9 (right panel) means to adjust all frequencies of occurrence of radar reflecticity of level 3 to approx. 3800 (see regression line) by using the correction factor $f_{cor} = -20.3$ and Eq. (5).

The correction algorithm was developed mainly for moderate and heavy rain, not considering light rain. But because of the fraction of light rain and especially its high frequency of occurrence it is indispensable to neglect these amounts. Therefore, the part of the altitude correction has to be extended for light rain. Especially snow in the winter months with smaller reflectivities than rain influences the decrease of the frequency of occurrence of light rain pixels with altitude. Instead of the correction factor of $f_{cor} = -20.3$ for moderate and heavy rain a factor of $f_{cor} = -12.9$ for light rain is derived. So the observed decrease of the frequency of occurrence of radar pixels with height is smaller for light rain.

The result of the altitude correction is a radar image with comparable frequencies of occurrence of radar reflectivities independent of the distance or height from the radar. Figure 10 (bottom-left panel) shows the result for Fig. 2 (middle panel) after the altitude correction for level 3, which obviously reveals significant differences. But still, clutter influence remains. Therefore, the second correction should solve this problem.

HESSD
9, 4703–4746, 2012

An application and a validation of the altitude correction and the following clutter correction and adjustment can be found in Sect. 6.

5.2 Correction of clutter effects

According to the results of the statistical analysis in Sect. 4 clutter is closely dependent on reflectivity. The lower the reflectivity of rain is, the more the influence of clutter dominates. The number of pixels, which are corrupted by clutter, decreases significantly when the reflectivity increases. Therefore the correction also has to depend on reflectivity.

First, a separation of corrupted and uncorrupted pixels is done for each reflectivity level class. As the frequencies of occurrence of radar reflectivities of level 5 and 6 are too low to be statistically analysed, the selection of corrupted pixels of level 4 is adopted for these heavy rain levels. This separation described in Sect. 3 is similar to the one used in Sect. 4 for level 1 using an empirical distribution technique.

The main aim of the correction is to preserve the reliable natural precipitation patterns. Two ways to deal with clutter affected pixels seems reasonable. The first one is an interpolation algorithm by values of pixels of the closer environment. The second one is a kind of adjustment, where frequencies of occurrence of radar reflectivities are shifted to a higher level.

If single pixels are affected by clutter the interpolation technique is used as these pixel values are not reliable and an adjustment of single pixels may lead to a high variability in space for other time-spans than the calibration period. The frequency of occurrence for these corrupted pixels is calculated by interpolation by the closer environment (10 to 20 km) of uncorrupted pixels.

Within spokes the pixels themselves are usually not corrupted. A part of the transmitting power of the radar-beam is shaded, which leads to an underestimation of reflectivity. So the patterns within spokes are reliable. As each pixel of one spoke is influenced by the same obstacle all these pixels are regarded combined. As a consequence the patterns are preserved by using a mean adjustment. For each ray (1°) of one spoke

HESSD
9, 4703–4746, 2012

the median of the frequency of occurrence of one reflectivity class is calculated and compared to the median of the frequencies of all uncorrupted pixels of the adjacent 20–30 rays. The ratio of the two medians is calculated, which then serves as a correction factor. These factors vary between 1.1 and 1.5. The two spokes east of the radar are falsified by departing or landing planes and must therefore be completely interpolated.

5.3 Adjustment

The adjustment is based on the DX-product and represents the third module of the statistical correction scheme. Here, rain amounts are compared instead of frequencies of occurrence. So the radar data has to be converted into rainrate by the threepart Z/R-relationship in Table 2. Then mean annual rain rates from radar data were adjusted to rain rates from rain gauges for the time-span 2004–2006.

The plain correction of altitude increases the frequency of occurrence of radar reflectivities. But the overestimation of radar reflectivities due to the influence of the Bright Band has to be taken into account. The Bright Band is able to increase the radar reflectivity up to 10 dBZ or more, which is approx. a factor of 5 regarding rain rate (Bartels et al., 2004). To overcome this problem, a stable adjustment to the mean rain rate of rain gauges was realised. For the adjustment only the 33 rain gauges within a distance of 30 to 60 km from the radar (group 1) are used. Radar pixels in this area are highly reliable as these pixels are not influenced by the clutter of the inner city of Munich, but are still very close to the radar site. The other rain gauges (group 2 and group 3) were used in Sect. 6 for evaluation. So the rain amounts of the 33 rain gauges were compared to the corresponding rain amounts derived from radar reflectivities (9-pixel-value) resulting in a mean factor.

For long time-spans (1 yr) the following assumption is made: this mean factor can also be used to correct the frequency of occurrence of radar reflectivities as the variability of the mean dropsize spectra of the annual rain amount is not able to change this mean correction factor significantly.

HESSD
9, 4703–4746, 2012

This factor is then simply divided by the frequency of occurrence of radar reflectivities. This factor was determined for the corrected radar data as well as for the uncorrected radar data as the problem of increased values by the Bright Band affects both data sets. For the uncorrected data a factor of 0.94 was determined whereas for corrected data a factor of 1.26 resulted (cf. Fig. 10, top-right panel). Regarding long-term-measurements a good mean consistency between measurements from radar and rain gauges becomes obvious. But this is the result of a slight overestimation of rain rate by radar data near the radar and an underestimation at longer distances from the radar. The Bright Band seems to be responsible for this overestimation to a huge extent. The adjustment is only reasonable in conjunction with the first and second module of the correction algorithm.

Figure 10 shows the results of the entire correction algorithm for the Munich weather radar of radar reflectivity level 3. The visual impression reveals now a relatively homogeneous distribution of radar reflectivities over the whole image but is still conserving meteorological-geographical induced minima and maxima of rain. The comparable frequencies of occurrence of radar reflectivities within the whole radar image are hints for an effective and successful correction. In order to prove the quality of the correction algorithm a comparison with rain rates from rain gauges was performed and results summarised in the following section.

6 Evaluation of the method

6.1 Application of the method

The annual rain rate derived from radar measurements (9-pixel-value) is opposed to the annual rain rate of rain gauges (group 2) of 2004 to 2006. The 76 measurements were further subdivided into five groups according to their distance from the radar (every 20 km) representing the probable modification of radar rain rate with distance from the radar.

HESSD
9, 4703–4746, 2012

Figures 11 and 12 show each step of correction of radar data in comparison to rain gauges.

Figure 11 shows scatter-plots of mean annual rain rates of radar measurements and measurements of rain gauges. The subdivision into 20-km-classes (range class) is arranged column-wise. Each panel represents one step of the correction algorithm, starting with the uncorrected data (a), adjusted radar data (b), additional altitude correction (c) and entire correction (d). Figure 12 shows the same comparison in a Box-and-Whisker-Diagram with five boxes starting with the 0–20 km-class. The boxes and whiskers mark the percential difference of radar measurements in comparison with the corresponding rain gauge measurements for each range class. The first diagram shows the uncorrected mean annual rain rates with a certain variablility in class 1 (inner 20 km). Radar measurements next to the radar site have to be handled with care because of different measuring effects, which may falsify radar data. In addition, huge parts of class 1 represent the city of Munich with possible clutter effects. Classes 2 and 3 represent the most reliable areas within the radar-coverage with an excellent consistency of mean annual rain rates of radar data and data from rain gauges. Classes 4 and 5 reveal a significant underestimation of rain rate by radar measurements. According to Fig. 12 a mean underestimation of 20 % in class 4 can be found whereas in class 5 the underestimation is twice as high as in class 4 (40 %). It can be attested, that the decrease of rain rate by radar measurements with distance from the radar is a measuring effect of the radar, whereas the rain rate based on rain gauges is independent from this distance.

With the mean factor adjustment the radar measurements were shifted to a lower rain rate level in Fig. 11b. For all classes a significant underestimation of rain rate derived by radar measurements results. The RMSE rises from 262.1 mm to 359.3 mm (cf. Table 3). The second diagram of Fig. 12 reveals mean underestimations between 20 % and 50 % by radar data. Without the subsequent correction modules this correction leads to an impairment of data quality. Using the adjustment factor of 0.94 for uncorrected data a slight improvement of the RMSE to 247.3 mm becomes obvious (not shown here).

HESSD
9, 4703–4746, 2012

After the altitude correction a significant improvement of the consistency of measurements from radar and rain gauges becomes apparent (cf. panel c) in Fig. 11. Especially range classes 4 and 5, where the altitude correction has the greatest impact on the rain rate, are improved, both visually and based on statistical values. The RMSE changes from 262.1 mm (uncorrected data) to 126.4 mm. The Box-and-Whisker-Diagram supports these results. The maximum deviation-range of the median of radar rainrates from the median of rain rates from rain gauges of each range class decreases from −40 % to +2 % (uncorrected data) up to −15 % to +3 %.

Figure 11d shows the results after the entire correction including the correction of spokes and cluttered pixels. The RMSE (118.3 mm) indicates the further improvement as the diagram itself visually does. The maximum deviation-range of the median of radar rain rates from the median of rain rates from rain gauges of each range class decreases to −5 % to +5 %. A comparison of the diagrams in panel d with the diagrams in panel a shows a significant improvement for all range classes. The greater the distance from the radar site the higher the deviations of rain rates between measurements from radar and rain gauges. But even at a distance of 80 to 100 km (class 5) the maximum range of deviation of mean rain rates is −28 % to +33 % for all 76 pairs of value. This appears to be a small range, taking into account that measurements from rain gauges are affected by measuring-problems with wind or snow and may therefore differ from radar measurements. In addition the geography of the Munich radar coverage is very difficult concerning measurements of rain rate.

6.2 Validation of the method

For the validation of the presented correction algorithm the same comparisons of mean annual rain rates from radar measurements and rain gauges are used, but for the time span 2007 to 2009 and for all available 91 pairs of value (group 3). This also includes pairs of values in areas where the rain rates do not seem reliable or where radar measurements are obviously disturbed by clutter effects and have therefore be interpolated by measurements in the closer vicinity. The very southern part within the

HESSD
9, 4703–4746, 2012

range of the Alps usually shows higher rain rates especially at higher altitudes. The interpolation does not take these effects into account, so a massive underestimation of rainrate by radar measurements in comparison to rain gauge data in this area is likely. A second area of falsification is the inner part of the radar coverage. Major parts of range class 1 cover the city of Munich with clutter problems. The results are presented in Figs. 13 and 14.

The three diagrams of Fig. 13 are comparable to those in Fig. 12 but for all pairs of value. Comparisons of rain rate from uncorrected radar data of the years 2007 to 2009 in the first diagram is opposed to corrected radar data (2007–2009) in the second diagram. The third diagram shows the identical comparison as diagram 2 but for the years 2004 to 2006.

The first diagram (left panel) of Fig. 13 reveals a high variance, which is not very astonishing as this comparison also includes questionable pairs of value. The variances in range class 1 reflect the disturbances mainly caused by the inner city of Munich. An excellent consistency of radar data and rain gauges exist for range classes 2 and 3. The modification of rain rates with distance from the radar becomes clearly apparent in classes 4 and 5.

Diagram 2 (middle panel) shows the result of the entire correction algorithm. A significant improvement becomes obvious, both visually and based on the RMSE, which decreases from 322.2 mm to 174.1 mm (cf. Table 4). As expected, some pairs of value show only poor consistency. Most of them are located in the alpine area where interpolated radar data is not able to reproduce the high rain rates measured by rain gauges. The boxes and whiskers of diagram 2 show comparable ranges as diagram 4 of Fig. 11 does.

In diagram 3 (right panel) the same 91 pairs of value are compared for the calibration period to get evidence which part of the impairment of the results are based on the additional pairs of value and which part is based on the new time span. Diagram 3 shows a higher impairment than diagram 2 does. The RMSE of the validation period (RMSE = 174.1 mm) is smaller than the RMSE of the calibration period

HESSD
9, 4703–4746, 2012

(RMSE = 234.6 mm). So the impairment is mainly induced by the additional pairs of value.

The correction of radar data in the validation period show comparable improvements, as the correction in the calibration period does. In conclusion, the validation verifies the possibility of adaption of the correction algorithm for other time-spans. For this validation time-span the results are even better than those of the calibration time-span. This is mainly due to the installation of a new signal-processor in 2004 that leads to a much better suppression of clutter effects and an advanced scan strategy with different radiation angles in 2007.

Figure 14 serves as a terminal visual validation of the results of the whole correction algorithm. It shows the mean annual rainrates derived from DX-radar-products before (left panel) and after the statistical corrections (right panel). The uncorrected radar data reveals comparable patterns as the PX-product (2000–2006) does, such as spokes or a decrease of rain rate with altitude (cf. Fig. 1, left panel). With the new signal processor the distribution of rain rates derived from uncorrected radar data differs from the frequency of occurrence patterns in Fig. 1. Additionally, clutter suppression is improved significantly.

The corrected image of Fig. 14 (right panel) shows the expected distribution of rain rates known from areal rain rates derived from point measurements. The highest rain amounts are measured in the Alps and on the fringe of the Alps decreasing to the north. The radar image still reveals some remains caused by clutter (e.g. City of Munich) or spokes.

7 Summary

We presented a statistical analysis of disturbances and the influence of measuring effects of long-term precipitation radar measurements. Based on these findings a stable, statistical correction algorithm was derived. A significant improvement is shown using

HESSD
9, 4703–4746, 2012

these corrections due to a comparison of radar DX-data with rain gauges on an annual basis.

The statistical analysis of radar data on a large temporal scale showed: Small systematical differences within a radar coverage, which may lead to recognizeable errors in longer time-series were detected by this statistical analysis. The consequences of beam-widening and increasing beam-height above ground with increasing range on the rain rate can be seen on a long-time range. The enormous influence of the Bright Band not only at single event-scale but statistically becomes apparent. According to these results, it is indispensable to include the correction of the Bright Band if you use radar data for a longer time range, for example as input for a hydrological model in the water balance mode.

The whole presented correction algorithm is only suitable for climatological or statistical analysis with a temporal resolution of at least 1 yr. This limits the possible application of this correction algorithm. The part of the correction algorithm for clutter and spokes correction is also suitable for smaller time scales or even for single radar-image corrections. But the main impact of this algorithm is due to the altitude correction which strongly depends on the Bright Band. The formation of the Bright Band is very variable in space and time. But the Bright Band should be negligible for heavy precipitation in convective cells as convective cells usually have a huge vertical homogeneity of rain. There are some hints for that effect within this analysis, but the frequency of occurrence of such high reflectivity levels is too low to be statistically robust. It may be concluded, that the altitude correction could also be applied for heavy rain at shorter temporal resolutions than one year.

The alternative for this statistical altitude correction is a Bright Band correction or the correction of the vertical profile of reflectivity on single radar images. The possible applications would be larger. But it is likely that on a large-time-scale remaining small differences are summed to larger errors on one hand and on the other hand such a correction would not include any clutter or spoke corrections.

HESSD
9, 4703–4746, 2012

References

Bartels, H., Weigl, E., Reich, T., Lang, P., Wagner, A., Kohler, O., and Gerlach, N.: Projekt RADOLAN - Routineverfahren zur Online-Aneichung der Radarniederschlagsdaten mit Hilfe von automatischen Bodenniederschlagsstationen (Ombrometer), Deutscher Wetterdienst, Hydrometeorologie, 2004.

Fabry, F. and Zawadzki, I.: Long-term radar observations of the melting layer of precipitation and their interpretation, J. Atmos. Sci., 52, 838–851, 1995.

Franco, M., Sanchez-Diezma, R., and Sempere-Torres, D.: Improvements in weather radar rain rate estimates using a method for identifying the vertical profile of reflectivity from volume radar scans, Meteorol. Z., 15, 521–536, 2006.

Haase, G., Gjertsen, U., and Bech, J.: Weather radar data quality in Northern Europe: beam propagation issues, AMS Conference on Radar Meteorology, Albuquerque, Canada, 2005.

Holleman, I.: Bias adjustment and long-term verification of radarbased precipitation estimates, Meteorol. Appl., 14, 195–203, 2007.

Joss, J. and Lee, R.: The application of radar-gauge comparisons to operational precipitation profile corrections, J. Appl. Meteorol., 34, 2612–2630, 1995.

Kitchen, M., Brown, R., and Davies, A. G.: Real-time correction of weather radar data for the effects of bright band, range and orographic growth in widespread precipitation, Q. J. Roy. Meteorol. Soc., 120, 1231–1254, 1994.

Koistinen, J.: Operational correction of radar rainfall errors due to vertical reflectivity profile, in Proc. 25th Conf. on Radar Met., AMS, 91–94, 1991.

Koistinen, J., Kuitunen, T., Pulkkinen, S., Hohti, H., and Kotro, J.: Derivation of extreme event mesoscale area-intensity return periods of rainfall based on a large sample of radar data, ERAD, Helsinki, Finland, 2008.

Krajewski, W. F., Vignal, B., Seo, B.-C., and Villarini, G.: Statistical model of the range dependent error in radar-rainfall estimates due to the vertical profile of reflectivity, J. Hydrol., 402, 306–316, 2010.

Overeem, A., Holleman, I., and Buishand, T.A.: Derivation of a 10-year radar-based climatology of rainfall, J. Appl. Meteorol., 48, 1448–1463, 2009.

Overeem, A., Buishand, T. A., Holleman, I., and Uijlenhoet, R.: Extreme-value modeling of areal rainfall from weather radar, Water Resour. Res., 46, W09514, doi:10.1029/2009WR008517, 2010.

HESSD
9, 4703–4746, 2012

Pedersen, L., Jensen, N., and Madsen, E.: Extreme rainfall statistics based on rain gauges and radar measurements, Extreme rainfall statistics based on rain gauges and radar.pdf, WRaH Grenoble, France, 2008.

Rudolph, J., Friedrich, K., and Germann, U.: Relationship between radar-estimated precipitation and synoptic weather patterns in the European Alps, J. Appl. Meteorol. Clim., 50, 944–957, 2011.

Sánchez-Diezma, R., Zawadzki, I., and Sempere-Torres, D.: Identification of the bright band through the analysis of volumetric radar data, J. Geophys. Res., 105, 2225–2236, doi:10.1029/1999JD900310, 2000.

Vignal, B., Andrieu, H., and Creutin, H.: Identification of vertical profiles of reflectivity from volume scan radar data, J. Appl. Meteorol., 38, 1214–1228, 1999.

Wagner, A., Seltmann, J., and Lang, P.: URBAS_Radar – a statistical approach to radar climatology, Abstr. 4th European Conference on Radar in Meteorology and Hydrology (ERAD4), 18–22 September 2006, ERAD Publ. Series Vol. 3, Barcelona, Spain, p. 61, 2006.

HESSD

9, 4703–4746, 2012

Table 1. Reflectivity levels of the PX-product.

Reflectivity [dBZ]	<19	19–27.9	28–36.9	37–45.9	46–54.9	>55
Level	1	2	3	4	5	6

HESSD
9, 4703–4746, 2012

Table 2. Threepart Z/R-relationship used to calculate rain rate from DX-radar-products.

Reflectivity [dBZ]	<36.5	36.5–44	>44
a	125	200	77
b	1.4	1.6	1.9

HESSD
9, 4703–4746, 2012

Table 3. RMSE for the comparison of radar and rain gauge data in Figs. 10 and 11.

	uncor[1]	cor-b[2]	cor-ba[3]	cor-bac[4]
RMSE [mm]	262.1	359.3	126.4	118.3

[1] uncorrected radar data,
[2] corrected radar data (bias/adjusted),
[3] corrected radar data (bias/adjusted, altitude),
[4] corrected radar data (bias/adjusted, altitude, clutter)

HESSD
9, 4703–4746, 2012

Table 4. RMSE for the comparison of radar and rain gauge data in Fig. 12.

	uncor* (2007–2009)	cor-bac**	cor-bac** (2004–2006)
RMSE [mm]	322.2	174.1	234.6

* uncorrected radar data,
** corrected radar data (bias/adjusted, altitude, clutter)

HESSD
9, 4703–4746, 2012

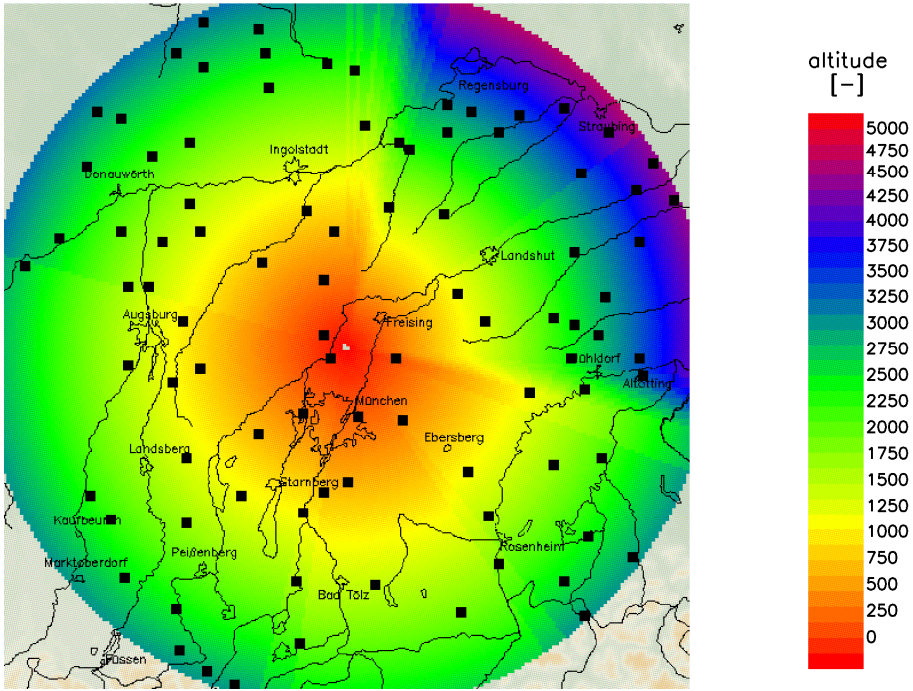

Fig. 1. Mean altitudes of the radar beam of the Munich Weather Radar (2000–2006). Overplotted by locations of the rain gauges used for comparing rain rates.

HESSD
9, 4703–4746, 2012

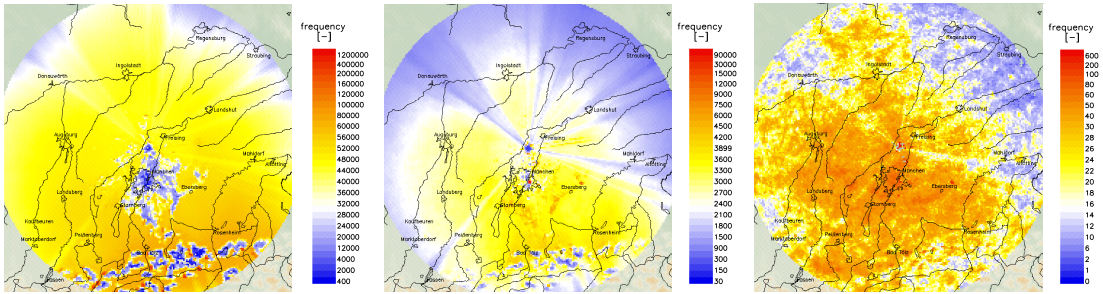

Fig. 2. Uncorrected frequencies of occurrence of radar reflectivity level 1 (left panel), level 3 (middle panel) and level 5 (right panel) of the Munich weather radar from 2000–2006.

HESSD
9, 4703–4746, 2012

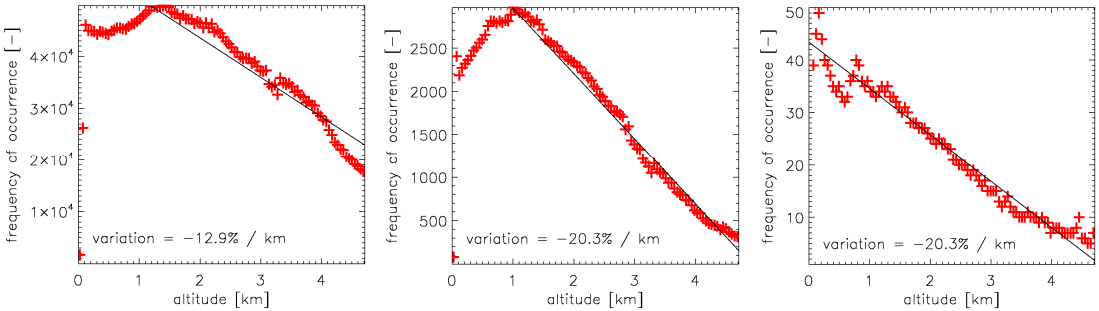

Fig. 3. Characteristics of the median of the frequency of occurrence of uncorrupted pixels with height for equidistant classes of altitude for the reflectivity levels 1 (left panel), 3 (middle panel) and 5 (right panel) of the Munich weather radar from 2000–2006.

HESSD
9, 4703–4746, 2012

Joint statistical correction of clutters and beam height for a radar climatology

A. Wagner et al.

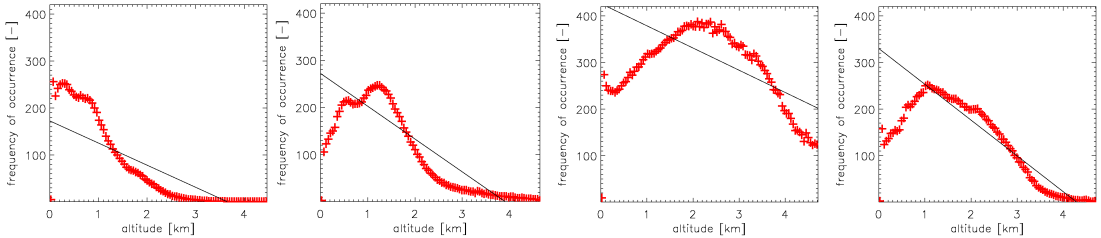

Fig. 4. As Fig. 3, but only for reflectivity level 3 separated into months showing January, April, July and October.

HESSD
9, 4703–4746, 2012

Joint statistical correction of clutters and beam height for a radar climatology

A. Wagner et al.

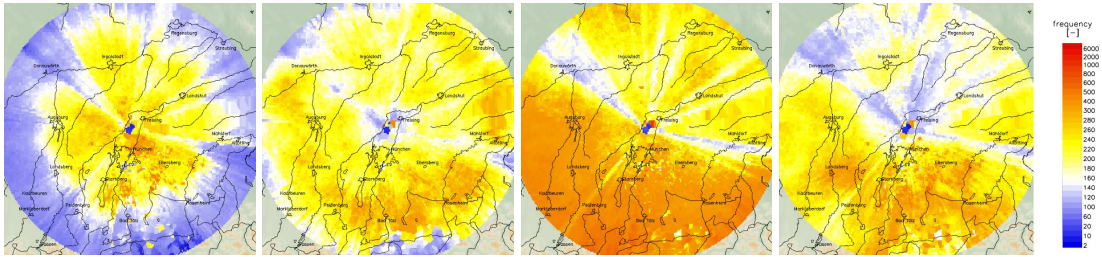

Fig. 5. Spatial distribution of the frequency of occurrence of radar pixels of level 3 of the Munich weather radar from 2000–2006 for January, April, July and October where all rays are reduced to the same maximum height.

HESSD
9, 4703–4746, 2012

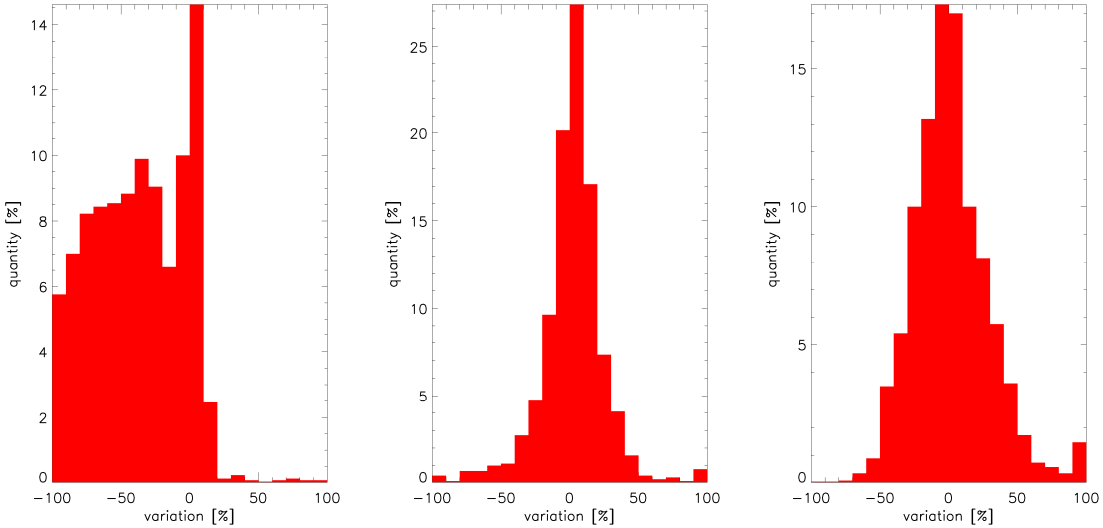

Fig. 6. Percential difference between the frequency of occurrence of city clutter pixels and the median of unfalsified pixels nearby for the reflectivity levels 1 (left panel), 3 (middle panel) and 5 (right panel) of the Munich weather radar from 2000–2006.

HESSD
9, 4703–4746, 2012

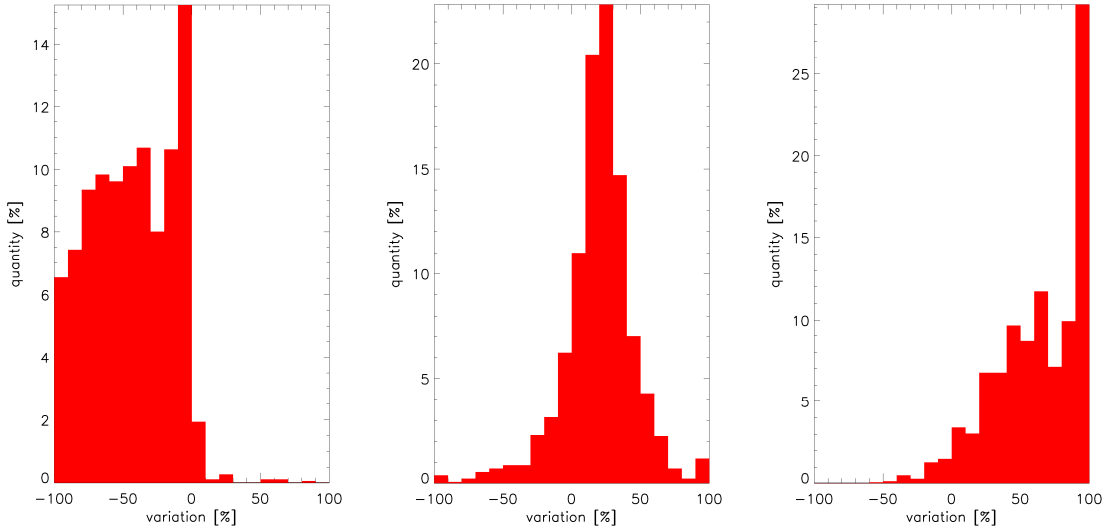

Fig. 7. As Fig. 6, but for mountain clutter for level 1 (left panel), 3 (middle panel) and 5 (right panel).

HESSD
9, 4703–4746, 2012

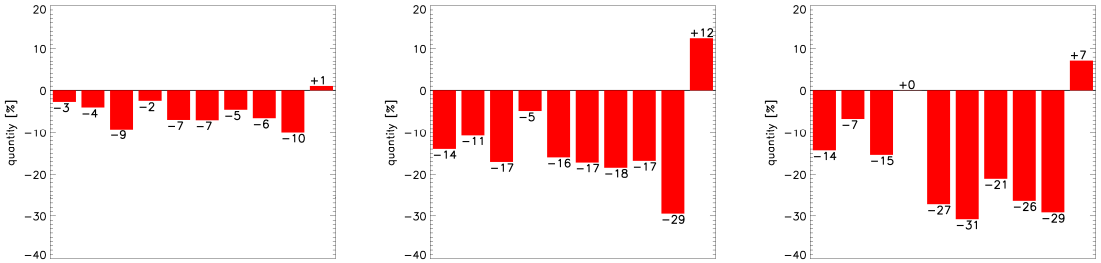

Fig. 8. Percential difference between the median of the frequency of occurrence of pixels within ten obvious spokes and the median of uncorrupted pixels nearby for the reflectivity levels 1 (left panel), 3 (middle panel) and 5 (right panel) of the Munich weather radar from 2000–2006.

HESSD
9, 4703–4746, 2012

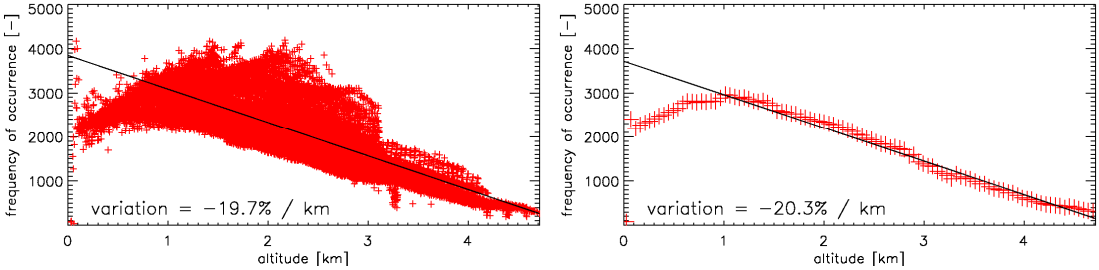

Fig. 9. Characteristics of the frequency of occurrence of uncorrupted pixels with height for the reflectivity level 3 of the Munich weather radar from 2000–2006 of all radar pixels (left panel) and of the median for equidistant classes of altitude (right panel).

HESSD
9, 4703–4746, 2012

Joint statistical correction of clutters and beam height for a radar climatology

A. Wagner et al.

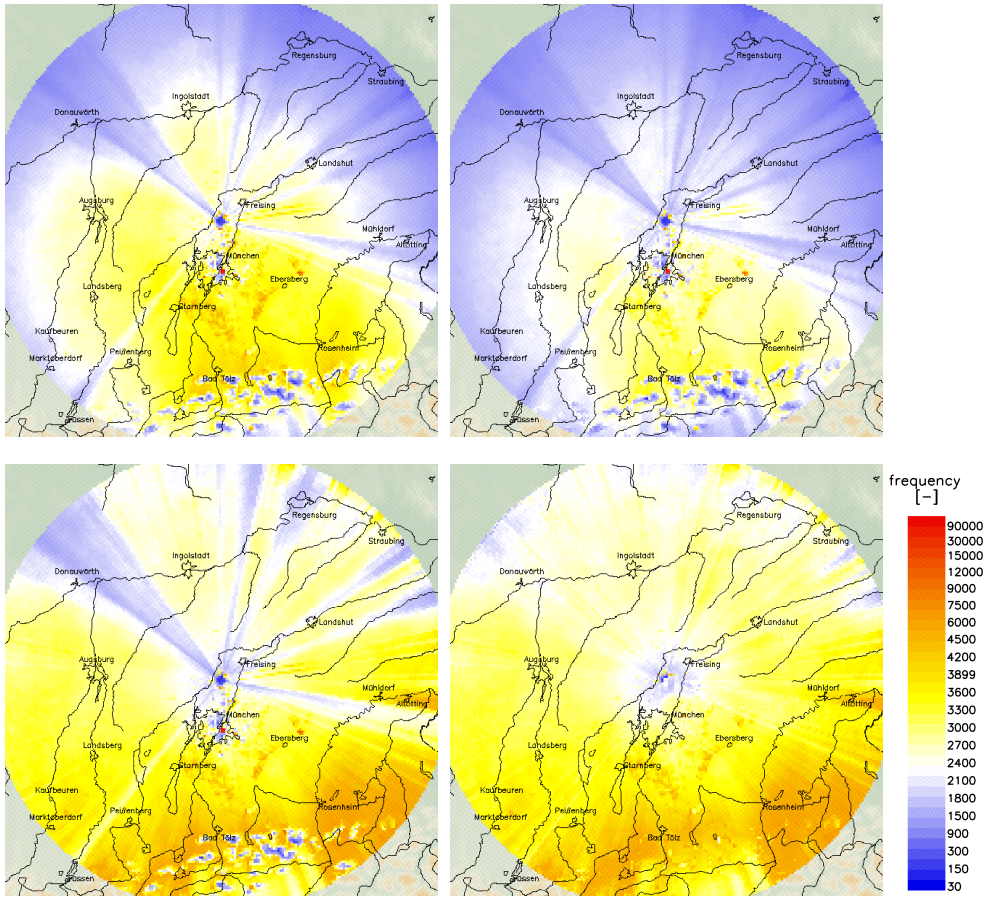

Fig. 10. Result of the statistical correction of the frequencies of occurrence of reflectivities (level 3) of the Munich weather radar from 2000–2006 – top left panel: uncorrected, top right panel: adjusted, bottom left panel: adjusted and altitude correction, bottom right panel: entire correction.

HESSD
9, 4703–4746, 2012

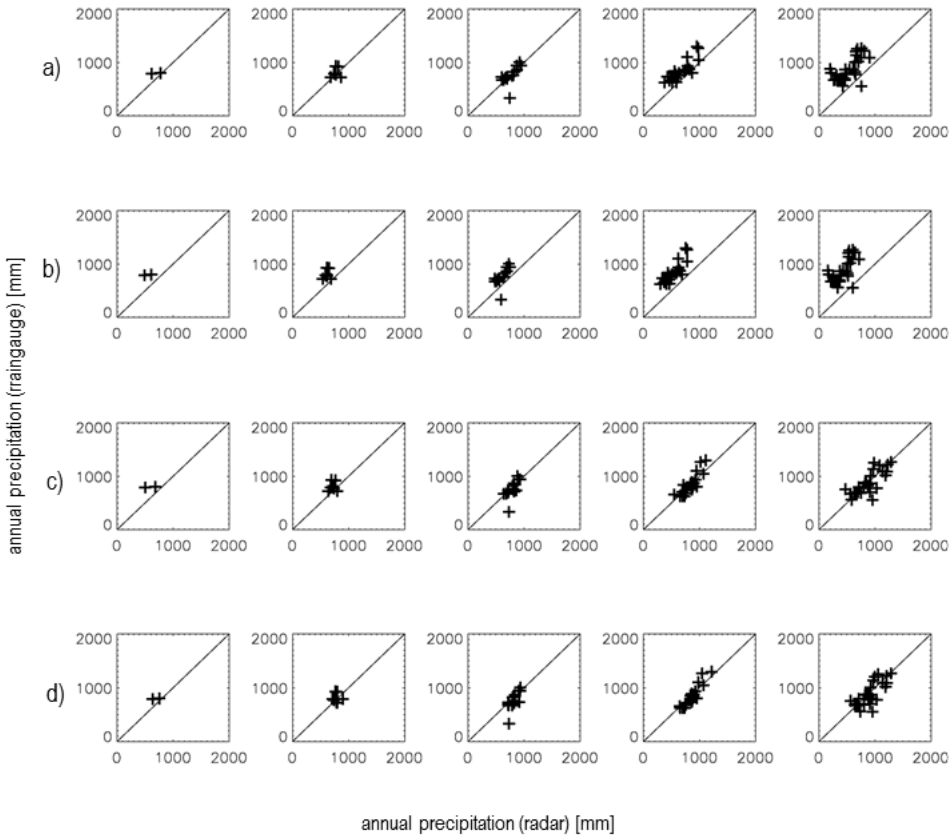

Fig. 11. Scatter-Plot of radar and rain gauge pair of values for the statistical correction of reflectivity level 3 of the Munich weather radar from 2000–2006. Each panel shows one step of the correction algorithm: **(a)** uncorrected, **(b)** adjusted, **(c)** adjusted and altitude corrected, **(d)** entire correction. The radar and rain gauge pair of values are subdivided into five classes according to their distance from the radar site. Each column represents one range class: 0–20 km, 20–40 km, 40–60 km, 60–80 km and 80–100 km.

HESSD
9, 4703–4746, 2012

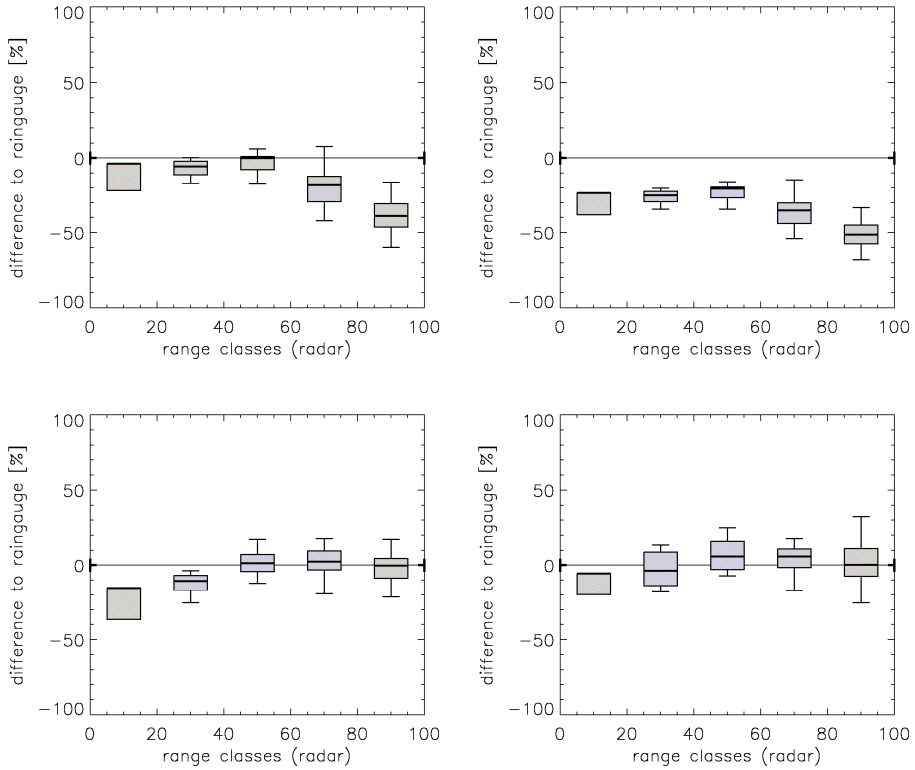

Fig. 12. Same data as for Fig. 11 but Box-and-Whisker-Diagram. The percential difference between radar data and rain gauge for each range class is shown. The thick bar indicates the median of each range class. The boxes show the deviation of 50 % of all radar and rain gauge pair of values of one class. The whiskers mark 1.5 times the corresponding interquartile range or, if not reached, the maximum deviation.

HESSD
9, 4703–4746, 2012

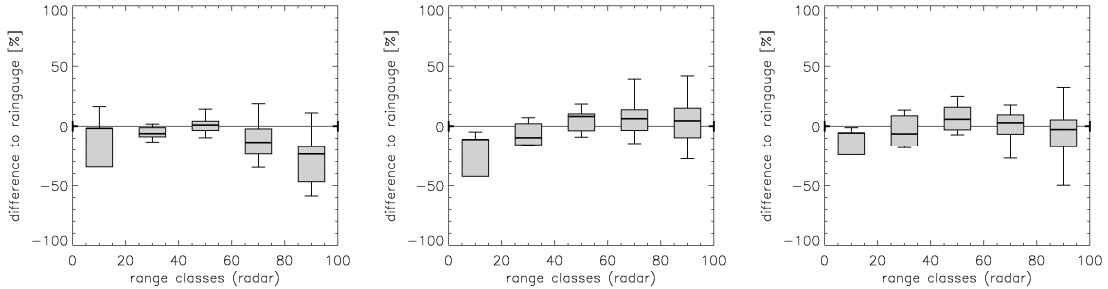

Fig. 13. Box-and-Whisker-Diagram of all radar and rain gauge pair of values for the statistical correction of reflectivity level 3 of the Munich weather radar – left panel: uncorrected (2007–2009), middle panel: entire correction (2007–2009), right panel: entire correction (2004–2006).

HESSD
9, 4703–4746, 2012

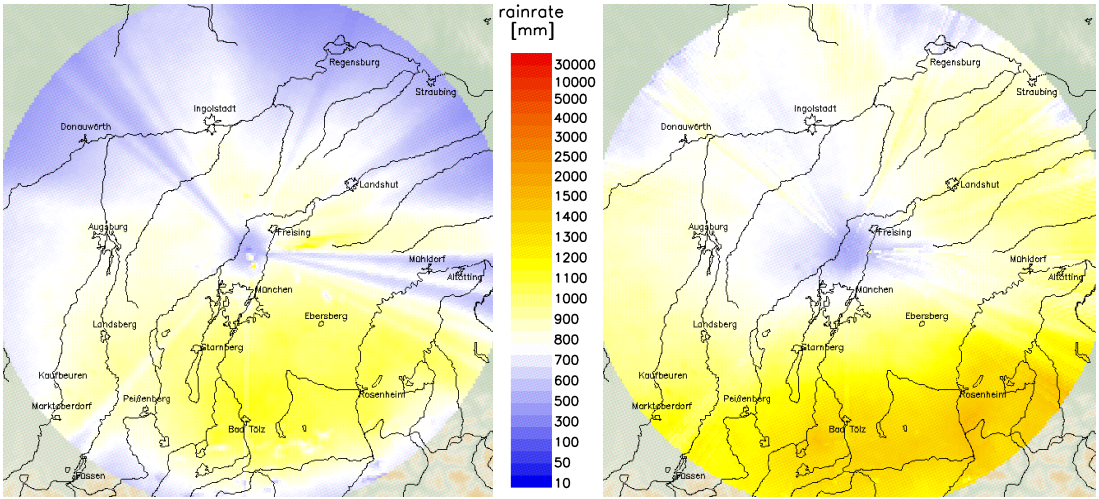

Fig. 14. Mean annual rain rate derived from the DX-radar-product of the Munich weather radar 2007–2009 – left panel: uncorrected, right panel: corrected.

HESSD
9, 4703–4746, 2012